Hunter, G.; Riedemann, J.; Andrade, I.; Blasco-Gimenez, R.; Peña, R. (2019). Power control of a grid-connected PV system during asymmetrical voltage faults. Electrical Engineering. 101(1):239-250. https://doi.org/10.1007/s00202-019-00769-x

Power Control of a Grid-Connected PV System During Asymmetrical Voltage Faults

Gustavo Hunter[1], Javier Riedemann[2], Iván Andrade[3], Ramón Blasco-Gimenez[4], Rubén Peña[1]

[1]Department of Electrical Engineering, Universidad de Concepción, Concepción, Chile
[2]School of Electrical Engineering, Pontificia Universidad Católica de Valparaíso, Valparaíso, Chile
[3]Department of Electrical Engineering, Universidad de Magallanes, Punta Arenas, Chile
[4]Department of Systems and Automatics, Universitat Politécnica de Valencia, Valencia, Spain

Corresponding author: Javier Riedemann (e-mail: javier.riedemann@pucv.cl – Phone: 56-32-2273680).

This work was funded by Conicyt Chile under project FONDECYT 11180092. The financial support given by CONICYT/FONDAP/15110019 is also acknowledged.

Abstract Under voltage faults, grid-tied photovoltaic inverters should remain connected to the grid according to fault ride-through requirements. Moreover, it is a desirable characteristic to keep the power injected to grid constant during the fault. This paper explores a control strategy to regulate the active and reactive power delivered by a single-stage photovoltaic generation system to the grid during asymmetrical voltage faults. The reference for the active power is obtained from a Maximum Power Point Tracking algorithm, whereas the reference for the reactive power can be set freely if the zero-sequence voltage is null, otherwise it will depend on the magnitude of the zero-sequence voltage and the active power reference. The power control loop generates the reference currents to be imposed by the grid-tied power inverter. These currents are regulated by a predictive controller. The proposed approach is simpler than other methods proposed in the literature. The performance of the control strategy presented is verified with an experimental laboratory setup where voltage sags and swells are considered.

Keywords Solar Power Generation, Current Control, Power Generation

Nomenclature

PV	:	Photovoltaic
MPPT	:	Maximum power point tracking
DC	:	Direct current
AC	:	Alternating current
P	:	Active power
Q	:	Reactive power
IARC	:	Instantaneous active reactive control
AARC	:	Average active reactive control
BPSC	:	Balanced positive sequence control
PNSC	:	Positive-negative sequence control
FRT	:	Fault ride-through
LVRT	:	Low voltage ride-through
PLL	:	Phase locked loop
VSC	:	Voltage source converter
LV	:	Low voltage
MV	:	Medium voltage
P&O	:	Perturb and observe
PCC	:	Point of common connection
THD	:	Total harmonic distortion
$\boldsymbol{v}_{abc}$	:	Voltage in abc reference frame
$\boldsymbol{v}_{\alpha\beta\gamma}$	:	Voltage in $\alpha\beta\gamma$ reference frame
$\boldsymbol{i}_{abc}$	:	Current in abc reference frame
$\boldsymbol{i}_{\alpha\beta\gamma}$	:	Current in $\alpha\beta\gamma$ reference frame
$\boldsymbol{i}^{*}_{\alpha\beta}$	:	Reference current in $\alpha\beta$ reference frame
$\boldsymbol{p}(\boldsymbol{t})$	:	Instantaneous active power
$\lvert[\boldsymbol{q}_{abc}]\rvert$	:	Instantaneous reactive power
$\mathbf{p}_{\mathbf{ref}}$	:	Active power reference
$\lvert\mathbf{q}\rvert_{\mathbf{ref}}$	:	Reactive power reference

1 Introduction

The increase in the world population and environmental pollution, along with the decrease in the fossil-based fuels, have made the renewable energy sources a very attractive alternative for electrical power generation. Nowadays, photovoltaic systems are the fastest growing and most promising renewable energy source in the world. It is estimated a worldwide PV installed power of about 871 GW in 2022 [1]. A photovoltaic module converts the solar irradiation into DC electrical energy; then to connect a PV system to the electrical grid, this DC voltage needs to be transformed into AC voltage by means of a power electronics converter. Moreover, to optimize the energy captured from the PV system, a Maximum Power Point Tracking (MPPT) algorithm [2] is always considered. In general, MPPT is a method to extract the maximum power available in a variable generation source (e.g. wind, solar, etc.), and for PV systems the most common MPPT techniques used are [2]: perturb & observe, incremental conductance and ripple correlation, among others. Moreover, intelligent

MPPT strategies based on fuzzy logic and neural networks can also be found in the literature [2]-[4].
Regarding the power conversion topology of a grid connected PV system, it can be classified in two types: 1) Single-stage: where there is only one DC/AC power converter with ability to handle all the tasks, i.e. MPPT and grid current control [5]-[6], 2) Multi-stage: where one or more DC/DC power converters are incorporated to carry out MPPT [7]-[8]. However, multi-stage systems have some drawbacks such as a lower reliability, higher cost, and larger size compared to single-stage systems [9], [10].

Independent of the number of stages considered for the energy conversion, the continuous and efficient operation of the system is fundamental even under the presence of abnormalities in the grid such as symmetrical/asymmetrical sags (reduction of voltage magnitude) and swells (increase in the voltage magnitude). In this sense, Fault Ride-Through (FRT), that is defined as "the ability of generating units to ride through transmission system faults and disturbances" [11], is a desirable characteristic in every power system [12]. Hence, the study of faults and FRT control in generation systems containing renewable sources (islanded or grid-tied topologies and microgrids) has been a matter of interest in last years.

In [13]-[15], control strategies for grid-tied power inverters during asymmetrical faults are proposed. The methods presented in [13]-[14] aim to reduce the DC-link voltage oscillations and the harmonic content of the currents injected to the grid during a fault. In [15] the aim is to minimize the peak value of the grid currents during the fault.

A FRT strategy that limits the fault current by using an adjustable resistor connected in the inverter DC-link, is presented in [16]. During normal operation the current limiter has no effect on the inverter operation, and during a fault, the adjustable resistor will limit the current in the faulty phases and does not affect healthy lines.

In [17], a model predictive control for a grid-connected inverter with FRT capability is presented. The control strategy is developed to obtain a constant DC-link voltage during the fault, however the active and reactive power injected to the grid do not remain constant.

Regarding the integration of PV and other renewable generation sources in grids/microgrids, the study of different types of faults and control techniques have been reported in literature. In [18]-[20] different methodologies to analyze unsymmetrical faults in microgrids are presented. In [21] it is carried out the application of neural network algorithms to control and improve the transient stability in a hybrid generation system; the aim is to reduce the power fluctuations and to provide voltage support during transient operation. In [22], it is presented a control strategy to limit the voltage and current during a fault in an islanded microgrid. The strategy is tested with symmetrical and asymmetrical faults showing good performance.

On the other hand, the control of active (P) and reactive (Q) power injected to the grid by PV systems, during unbalanced voltage faults, have been also widely studied. In [23]-[24] a review of four grid fault control strategies is presented: (1) Instantaneous active reactive control (IARC), (2) average active reactive control (AARC), (3) balanced positive sequence control (BPSC) and (4) positive-negative sequence control (PNSC). The general principle of the above techniques is to decompose the measured grid voltage into positive and negative sequence. Then, the control strategy calculates the current reference during a voltage fault by using one or both sequence components. The current reference based on IARC contains harmonics whereas AARC, BPSC and PNSC strategies give rise to output power fluctuation. A control method that maximizes the power capability of the inverter, by injecting the maximum rated current during voltage sags containing positive and negative sequences voltages, is presented in [25]. The strategy combines a balance between positive and negative sequences currents, limiting the inverter output current to the maximum rated value and avoiding active power oscillations. In [26] a control system based on a fuzzy neural network is developed for active/reactive power control of a PV system which complies with the Low Voltage Ride Through (LVRT) regulations under grid faults containing positive and negative sequences voltages, without exceeding the maximum current limit.
Whereas most previous works have considered the use of negative sequence currents to regulate active and reactive current references during unbalanced faults, the effects of zero-sequence voltages have been addressed in [27] where simulations results have been presented.

This paper presents an experimental implementation to obtain a real-time validation of the control strategy presented in [28], intended to inject the desired active/reactive power during asymmetrical voltage sags and swells in a single-stage PV system.

The reference currents to be injected to the grid are obtained from the reference powers and the measured grid voltage. Then, the currents are controlled by a model predictive control (MPC) strategy [29], taking advantage of the features offered by this technique such as: straightforward implementation and capability to deal with non-linearities, among others. Although MPC has been used in PV systems [17],[30]-[31], it has not been used in a power control scheme such as presented in this article. Then, the combination of a power control stage that generates reference currents to be imposed by a predictive controller in the converter output, operating in

a FRT strategy, is highlighted as an important contribution of this work.

Moreover, another important feature of the control strategy proposed is that avoids the need of a Phase Locked Loop (PLL) scheme for grid synchronization purposes [32]-[33], then facilitating the management of this task.

In this work, faults containing positive, negative and zero sequence voltages are considered. It is shown that under the presence of zero sequence voltage faults, a restriction for the active and reactive power injected to the grid needs to be fulfilled in order to control the power to the desired value without power oscillation. The strategy is experimentally verified considering a single-stage inverter and an emulated PV system.

The paper is organized as follows. Section 2 presents the topology proposed with the description of the hardware elements, the MPPT method used and the control strategy. Section 3 presents the experimental results from a laboratory setup. Section 4 gives the conclusions.

2 Photovoltaic system

A large PV plant with centralized configuration is shown in Fig. 1. The PV array is connected to the grid by a Voltage Source Converter (VSC) that is responsible of MPPT as well as controlling active and reactive power injection. The PV arrays, consisting on several modules connected in series, operate at less than a 1 kV hence a transformer is used to increase the Low Voltage (LV) operation to a Medium Voltage (MV). Then, the electrical energy is transmitted to a substation where a power transformer elevates the voltages from medium to high voltage for large distance transmission purposes. The grid-connected photovoltaic system used in this work is represented in Fig. 2, where the different control variables and the Point of Common Connection (PCC) are shown. The PV module array is connected to a single grid. For simplicity, only an inductive filter (L filter) is connected between the power inverter and the grid, instead of LC or LCL filter configurations [34]. However, as can be appreciated in the experimental results shown in Section 3, this consideration does not affect the performance of the proposed strategy. Fig. 3 shows the control scheme for the grid-connected photovoltaic system. This control system can be separated into three stages: PV panel and MPPT method; reference currents calculation; and current control of the grid-tie inverter.

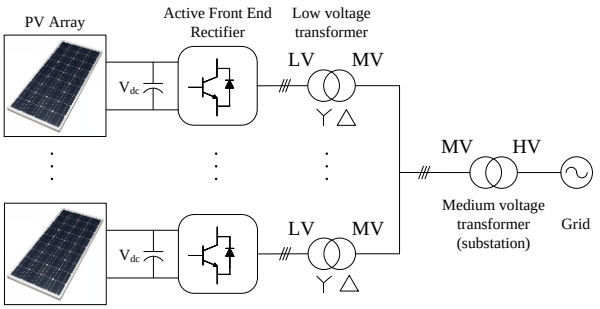

Fig. 1 Typical PV plant connected to the grid

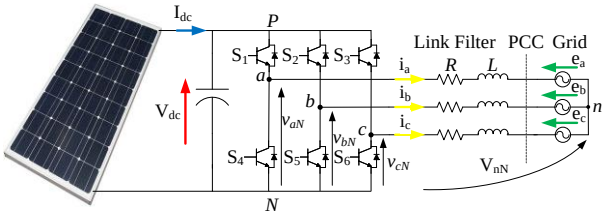

Fig. 2 Grid-connected photovoltaic system

2.1 PV panel and MPPT method

A PV array consists of several photovoltaic modules connected in series and parallel, which define the maximum power voltage (V_{MPPT}) and current (I_{MPPT}), the short circuit current (I_{SC}) and open circuit voltage (V_{OC}). In this work, a commercial PV panel from the company Sunedison model D330 is considered. The parameters of this panel at standard test conditions (1000 W/m2 and 25°C), are $I_{MPPT} = 8.77\ A$, $V_{MPPT} = 37.7\ V$, $I_{SC} = 9.28\ A$ and $V_{OC} = 46.2\ V$.

On the other hand, as aforementioned, MPPT is a strategy to extract the maximum available power in the PV array. Among the several MPPT methods proposed in the literature [2], [35], the most known are:

- Perturb and observe (P&O): method that operates periodically incrementing or decrementing the output voltage of the PV array and comparing the power obtained in the current cycle with the power of the precious cycle. P&O is the most widely used MPPT method due to its very easy implementation and low computation requirements. However, it has the drawback of wrong MPP tracking during fast changes in solar irradiation.

- Incremental conductance (IC): method based on the fact that the power slope of the PV is null at MPP, positive in the left and negative in the right. Due to this condition, the MPP can be found in terms of the increment in the array conductance.

- Ripple correlation (RC): strategy that makes use of the current or voltage ripples inherent in power converters, as these ripples provide some information about the system operating point. RC has the advantage

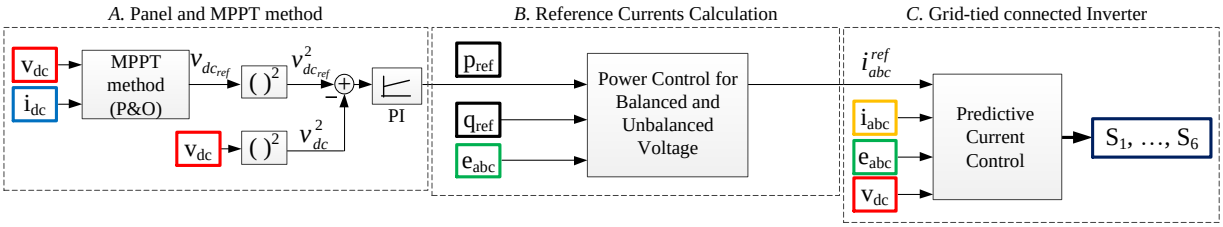

Fig. 3 Control scheme for grid-connected photovoltaic system for balanced and unbalanced grid voltage conditions

of not introducing any external disturbance into the system but makes use of the current or voltage ripple already present in the system. In this work, for the sake of simplicity, the MPPT method used is P&O. Moreover, as it will be considered that during a fault the solar irradiation will not suddenly change, it is expected a good performance of P&O method along with the FRT strategy proposed. The parameters considered for P&O are [36]: tracking speed=5s and voltage step=5V. A Proportional-Integral (PI) controller is used to process the DC voltage error and generate the power reference for the inverter (Fig. 4). The controller parameters used in this work, for a closed loop natural frequency of 10 Hz and a damping ratio of 0.707, are $k_p = 0.1091$, $k_i = 4.7418$ with $C = 470\ \mu F$.

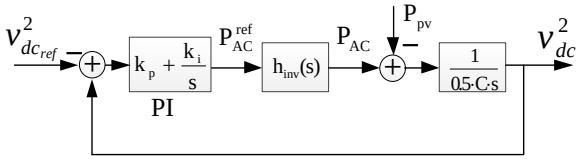

Fig. 4 DC-link voltage control loop

2.2 Reference current calculation

The aim of the proposed strategy is to control the active and reactive power supplied to the grid by the power converter during asymmetric voltage disturbances. The method assumes that the instantaneous active/reactive power references and grid voltage are known.

Considering the grid voltage and current in abc coordinates $[v_{abc}] = [v_a \quad v_b \quad v_c]^t$ and $[i_{abc}] = [i_a \quad i_b \quad i_c]^t$, then the active power is obtained as $p(t) = [v_{abc}]^t \cdot [i_{abc}]$. Using Clarke's transformation, presented in (1):

$$T_{abc\to\alpha\beta\gamma} = T = \frac{2}{3}\begin{bmatrix} 1 & -\frac{1}{2} & -\frac{1}{2} \\ 0 & \frac{\sqrt{3}}{2} & -\frac{\sqrt{3}}{2} \\ \frac{1}{2} & \frac{1}{2} & \frac{1}{2} \end{bmatrix} \tag{1}$$

and defining $[v_{abc}] = T^{-1}[v_{\alpha\beta\gamma}]$and $[i_{abc}] = T^{-1}[i_{\alpha\beta\gamma}]$ then the instantaneous active power in $\alpha\beta\gamma$ coordinates is given by:

$$p(t) = \left(T^{-1}[v_{\alpha\beta\gamma}]\right)^t \cdot \left(T^{-1}[i_{\alpha\beta\gamma}]\right) \tag{2}$$

$$p(t) = [v_{\alpha\beta\gamma}]^t (T^{-1})^t \cdot (T^{-1})[i_{\alpha\beta\gamma}] \tag{3}$$

Since $i_a + i_b + i_c = 0$, then the instantaneous power is calculated by (4).

$$p(t) = \frac{3}{2} v_\alpha i_\alpha + \frac{3}{2} v_\beta i_\beta \tag{4}$$

This is a well-known expression due to the absence of zero sequence current. Therefore, during a fault condition any zero-sequence voltage does not affect the calculation of the active power. The instantaneous reactive power is obtained as: $|[q_{abc}]| = |[v_{abc}] \times [i_{abc}]|$ and using $[v_{abc}] = T^{-1}[v_{\alpha\beta\gamma}]$ and $[i_{abc}] = T^{-1}[i_{\alpha\beta\gamma}]$, yields to [37]:

$$|[q_{abc}]| = \left|\left(T^{-1}[v_{\alpha\beta\gamma}]\right) \times \left(T^{-1}[i_{\alpha\beta\gamma}]\right)\right| \tag{5}$$

that can be rewritten as:

$$|[q_{abc}]| = |T^{-1}|\left|T^t[v_{\alpha\beta\gamma}] \times [i_{\alpha\beta\gamma}]\right| \tag{6}$$

Developing (6), the expression for the instantaneous reactive power is given by (7) as function of the $\alpha\beta\gamma$ voltage and current components (in this case the zero-sequence current component is zero):

$$|[q_{abc}]| = \frac{3}{2}\sqrt{2v_\gamma^2\left(i_\alpha^2 + i_\beta^2\right) + \left(v_\alpha i_\beta - v_\beta i_\alpha\right)^2} \tag{7}$$

The reference currents needed to inject a certain active and reactive power to the grid is obtained using (4), (7) and defining $P = \frac{2}{3} p_{ref}$ and $Q = \frac{2}{3}|q_{ref}|$ as:

$$i_{\alpha1}^*, i_{\alpha2}^* = \frac{P v_\alpha \mp v_\beta \sqrt{\frac{-2P^2 v_\gamma^2 + Q^2(v_\alpha^2 + v_\beta^2)}{2v_\gamma^2 + v_\alpha^2 + v_\beta^2}}}{v_\alpha^2 + v_\beta^2} \tag{8}$$

$$i_{\beta1}^*, i_{\beta2}^* = \frac{P v_\beta \pm v_\alpha \sqrt{\frac{-2P^2 v_\gamma^2 + Q^2(v_\alpha^2 + v_\beta^2)}{2v_\gamma^2 + v_\alpha^2 + v_\beta^2}}}{v_\alpha^2 + v_\beta^2} \tag{9}$$

It can be observed from (8)-(9) that there are two possible sets of reference currents. The first set, $i_{\alpha1}^*$, $i_{\beta1}^*$,

corresponds to lagging power factor operation, whereas the second set $i^*_{\alpha 2}$, $i^*_{\beta 2}$ corresponds to leading power factor operation. Both solutions must satisfy the following restriction: $\frac{-2P^2v_\gamma^2+Q^2v_\alpha^2+Q^2v_\beta^2}{2v_\gamma^2+v_\alpha^2+v_\beta^2} \geq 0$. Hence, in order to obtain reference currents with physical meaning, the desired active and reactive power p_{ref} and q_{ref} must satisfy the following condition:

$$|q|_{ref} \geq \frac{\sqrt{2}v_\gamma}{\sqrt{v_\alpha^2+v_\beta^2}} p_{ref} \tag{10}$$

The unbalanced voltage faults produced between the PV inverter and the PV plant transformer could generate zero sequence voltages. Therefore, the restriction in (10) needs to be satisfied for the system to be able to inject the desired active and reactive power.

2.3 Grid-tied inverter

Fig. 2 shows the VSC connected to a three-phase voltage supply through a filter inductance L with resistance R. The model of the system in abc coordinates is given in (11)-(13).

$$V_{aN}(t) = L\frac{di_a(t)}{dt} + Ri_a(t) + e_a(t) + V_{nN}(t) \tag{11}$$

$$V_{bN}(t) = L\frac{di_b(t)}{dt} + Ri_b(t) + e_b(t) + V_{nN}(t) \tag{12}$$

$$V_{cN}(t) = L\frac{di_c(t)}{dt} + Ri_c(t) + e_c(t) + V_{nN}(t) \tag{13}$$

Using (1), the system model is transformed into $\alpha\beta\gamma$ coordinates, where gamma component reflects the zero-sequence voltage.

To impose the reference currents by the grid-tied inverter, a predictive current control scheme is used [38]. Hence, a discrete model in $\alpha\beta$ coordinates is necessary to estimate the currents in the sampling instant $k+2$. These currents will depend on the converter voltage vector and the grid voltage and current values [39]. The error between the reference and the measured current is minimized by evaluating the following cost function for all the possible switching states (voltage vectors) of the grid-tied inverter.

$$g = \left|i^*_\alpha(k+2) - i^p_\alpha(k+2)\right| + \left|i^*_\beta(k+2) - i^p_\beta(k+2)\right| \tag{14}$$

Using Euler's approximation for calculating the derivative ($\frac{di}{dt} \approx \frac{i(k+2)-i(k+1)}{T_s}$), the discrete model of the system in $\alpha\beta$, is given by (15). It should be emphasized that Euler's approximation will give sufficiently accurate values for the predicted currents as the sampling period considered (56µs) is very low compared to the L/R time constant.

$$i^p{}_{\alpha\beta}(k+2) = \left(1 - \frac{RT_s}{L}\right)\hat{\imath}_{\alpha\beta}(k+1) + \frac{T_s}{L}\left(v(k+1) - \hat{e}(k+1)\right) \tag{15}$$

$i^p{}_{\alpha\beta}(k+2)$: Predicted current of the system in $\alpha\beta$
$\hat{\imath}_{\alpha\beta}(k+1)$: Estimated current of the system in $\alpha\beta$
$v(k+1)$: Voltage applied by the inverter in $\alpha\beta$
$\hat{e}(k+1)$: Estimated voltage grid in $\alpha\beta$
R : Line resistance
T_s : Switching period
L : Line inductance

To calculate the vector to apply in $k+1$ instant, it is necessary to know the voltages and reference currents at sampling time $k+1$ and $k+2$ respectively. In order to do that, a Lagrange extrapolation function is used. The voltage and current estimations are given by:

$$\hat{e}(k+1) = 3\hat{e}(k) - 3\hat{e}(k-1) + \hat{e}(k-2) \tag{16}$$

$$i^*(k+2) = 6i^*(k) - 8i^*(k-1) + 3i^*(k-2) \tag{17}$$

As can be noted in (15), the predictive equation depends on the line R-L parameters. It is known that the resistance varies with temperature, which in turn depends on the current that can vary largely from zero to its rated value. However, despite this, as the sampling period used is low enough (56µs), variations on the line resistance (and/or inductance) will not affect considerably the prediction equation nor the performance of the overall control strategy.

A flow chart summarizing the control method proposed is shown in Fig. 5.

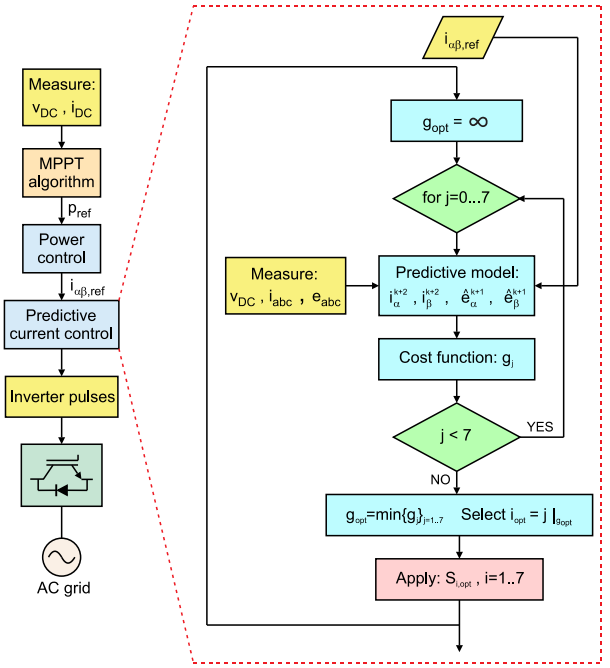

Fig. 5 Flow chart of the control strategy proposed

2.4 Limitations of the proposed method

The restriction shown in (10) indicates the ratio between active and reactive power to ensure the existence of reference current at any time. When the voltages are balanced, q_{ref} can take any value (even zero), but when an asymmetrical fault takes place, there will appear a voltage component v_γ and the restriction must be satisfied. In Fig. 6 it is shown the curves of $|q_{ref}|/p_{ref}$ (in blue) and the power factor (in black), as functions of a coefficient ρ, considering that the voltage in one phase is perturbed in magnitude as $V = (1-\rho)V_{rated}$. With this definition it is considered a swell when $-1 \leq \rho < 0$, and a sag when $0 \leq \rho \leq 1$.

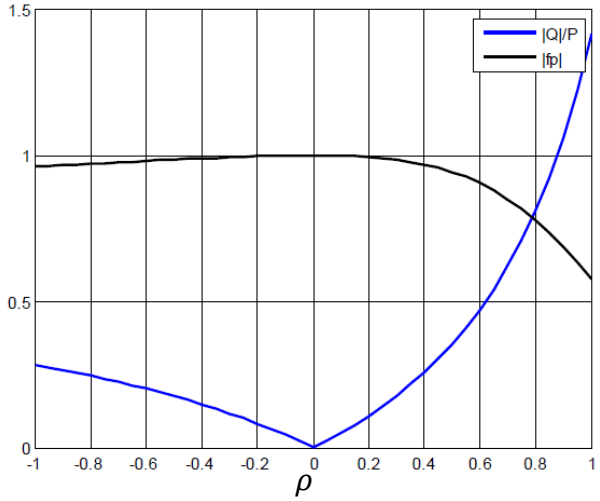

Fig. 6 Restriction for a fault in one phase

From Fig. 6 it is concluded that when a phase voltage doubles its normal magnitude, the relation $|q_{ref}|/p_{ref}$ equals $\frac{\sqrt{2}}{5}$. On the other hand, when a phase voltage is zero, the quotient between reactive and active power must be greater than $\sqrt{2}$. It is also evident that during a sag the system will operate with a power factor lower than during a swell, and it is not possible to operate with unity power factor during a fault if active and reactive power are kept constant.

In Fig. 7 it is shown the relation between active and reactive power when a fault occurs in two phase voltages simultaneously. In this case it is assumed that the voltage magnitude in one phase is $V_1 = (1-\rho_1)V_{1,rated}$ and in another phase is $V_2 = (1-\rho_2)V_{2,rated}$, with $\{\rho_1, \rho_2\} \in [-1,1]$.

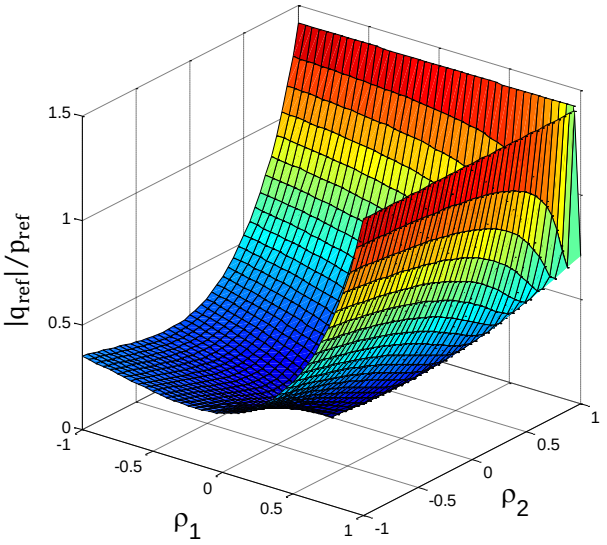

Fig. 7 Restriction for a fault in two phases

In conclusion, the relation (10) must be satisfied in order to maintain constant the magnitude of active and reactive power injected to the grid during a fault. Moreover, another limitation of the method proposed is that (10) only ensures the existence of reference currents to obtain constant P and Q during a fault, but it does not give information if these currents would have peak values greater than admissible by the power inverter, or high values of Total Harmonic Distortion (THD).

3 Experimental results

Experimental results are obtained from a 2.5 kW laboratory set-up, shown in Fig. 8. The PV panels are emulated by means of a Magna Power SL600-4.3 PV emulator with $I_{MPPT} = 4.05\,A$, $V_{MPPT} = 32.7\,V$, $I_{SC} = 4.3\,A$ and $V_{OC} = 40\,V$. The Analog-to-Digital conversion system and the voltage vector timing for the inverter are generated by an Actel A3P400 FPGA controlled by a TMSC6713 DSP. The communication between the DSP and Matlab platform is carried out by a Host Port Interface (HPI) daughter card. The voltage grid is set by a three-phase autotransformer. The fault (voltage sag or swell) is implemented with a single-phase autotransformer which adds and additional voltage (positive or negative) to phase-b. The system parameters are shown in Table 1.

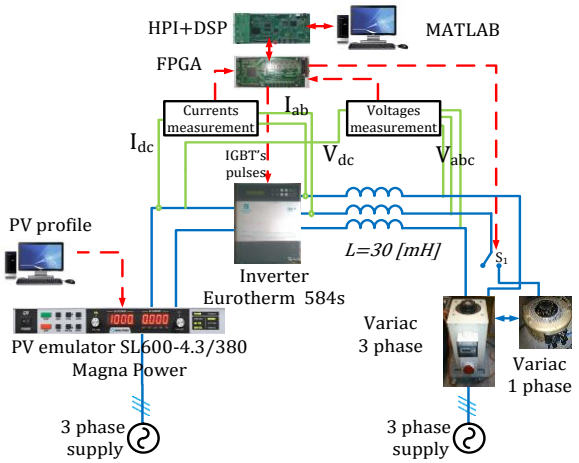

Fig. 8 Set-up for experimental results

Table 1. Experimental Parameters

R-L	0.25 Ω / 30 mH
C (VSC)	470 µF
V_{rms}	245 V
N_{series} / $N_{parallel}$	15 / 1 panels
T_s	56 µs
f	50 Hz

Experimental results for normal operation of the PV system, with no grid faults, are presented in Fig. 9. The PV system is operating with a 220 V grid voltage. Initially, the irradiation and temperature for the system are 1000 W/m^2 and 25 °C. Both are stepped down to 700 W/m^2 and 40 °C, respectively and then return to the initial conditions. Irradiation and temperature are kept constant for 200 s between steps.

The DC voltage is shown in Fig. 9 (top). The power extracted from the panel is shown in Fig. 9 (middle). For normal conditions, the reactive power injected to the grid is zero, and the active power injected depends on the solar irradiation and panel temperature. The active and reactive powers are shown in Fig. 9 (bottom).

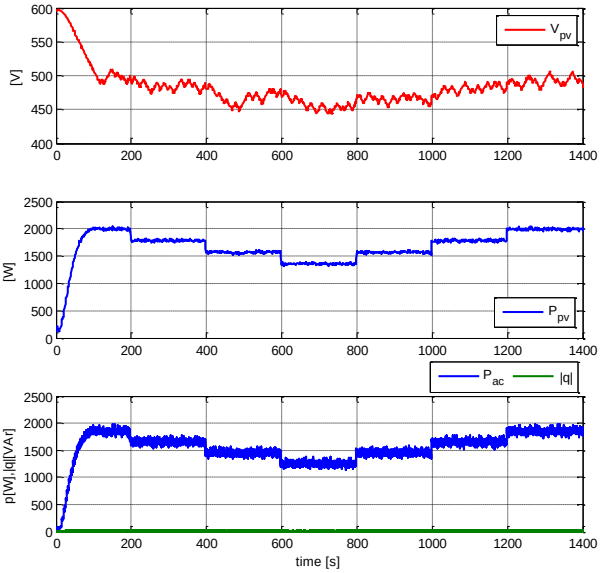

Fig. 9 Voltage PV (top), active power from PV array (middle) and active/reactive power (bottom) for normal operation

Initially, the DC voltage is 600 V. Under the MPPT algorithm the voltage settles within 505 V and 495 V. Initially the PV power is 200 W and settles at 2 kW. The PV array voltage and power settle to different values according to the MPPT for the corresponding irradiation and temperature profiles emulated. The PV voltage presents a ripple of 5 V due to MPPT action. The power injected to the grid varies accordingly with a 0.1 kW ripple. The power difference between dc and ac power is due to system losses.

Fig. 10 shows the $\boldsymbol{P_{dc}}$ vs $\boldsymbol{V_{dc}}$ curves for the different irradiation and temperature steps. It can be observed that the system tracks and remains at the MPP (in red) for each profile of irradiation and temperature.

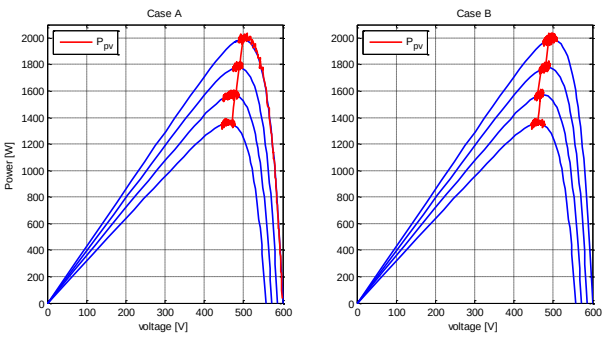

Fig. 10 MPPT method. a) During 0 and 800s b) During 600 and 1400s

3.1 Voltage sag: 40% phase B

The system is initially operating under normal conditions with irradiation of 1000 W/m^2 and 25°C. The reactive power reference is set to zero. The running time of the experiment is 0.2 s and a voltage sag of 40% in phase B

is applied from t=0.05 s to t=0.15 s (see Fig. 11 top). The grid fault contains a zero-sequence voltage and the restriction in (10) is not fulfilled. Fig. 11 (middle) shows the currents in the system. Before the fault, the RMS current is 4.7 A and 1.98 kW are injected to the grid. During the sag the RMS current reaches 7.1 A and the active power is regulated in 1.98 kW. However, the reactive power shows a ripple of 100 Hz with a peak of 0.5 kVAr.

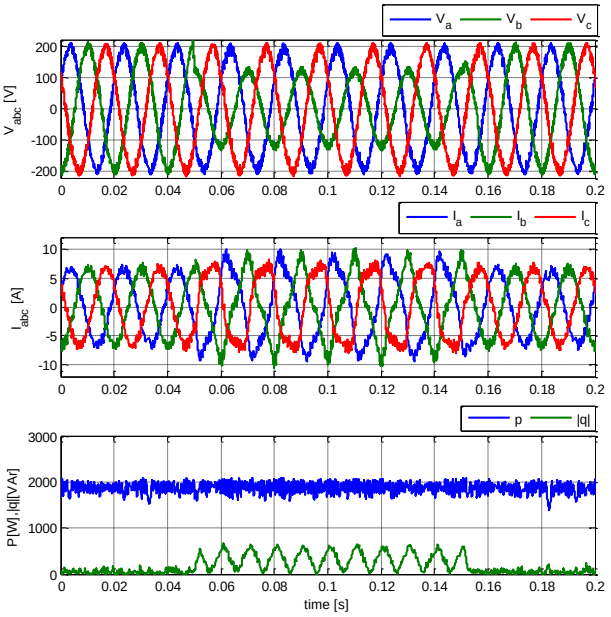

Fig. 11 Grid current (top) and active/reactive power injected (bottom) during a voltage sag

Fig. 12 shows the voltage and power delivered by the PV array. Before the sag the DC voltage is 495 V and 2 kW are generated. During the fault the array voltage shows a ripple of 100 Hz and 8 V whereas the active power remains constant through the experiment.

The THD for each current is calculated resulting in $THD_{i_a} = 19.2\%$, $THD_{i_b} = 22.9\%$ and $THD_{i_c} = 21.8\%$. During the fault, the current harmonic components are shown in Fig. 13.

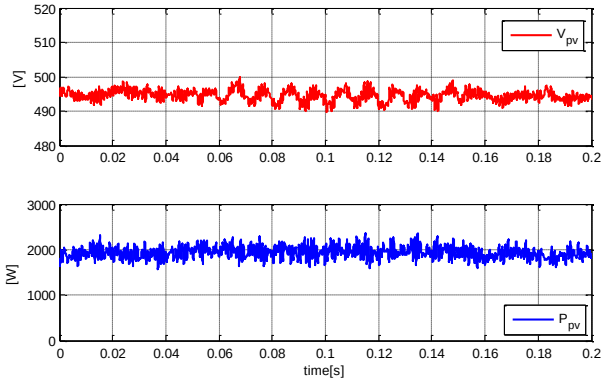

Fig. 12 Voltage (top), power for PV array (bottom) during a voltage sag

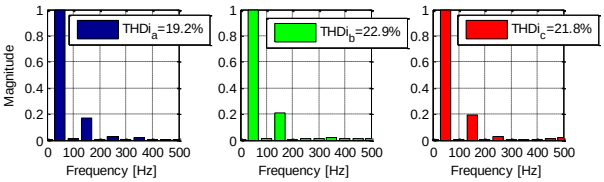

Fig. 13 Harmonic spectrum and THD for the currents during a sag

Another test considering a reference of 500 VAr for the reactive power is set with the same running time, irradiation, temperature and fault conditions of the previous experiment, to ensure the constraint in (10) is fulfilled for the considered 1.98 kW in active power. Fig. 14 shows the grid voltage, current and active/reactive power injected to the grid. The RMS current before the fault is 4.8 A with 1.98 kW injected to the electric system whereas the reactive power is 500 VAr. During the grid fault active and reactive power maintain their values. Fig. 15 shows the voltage and power delivered by the PV array. The dc voltage ripple is the same as in the previous test. The power delivered from the PV array remains unchanged.

The THD for each current is calculated resulting in $THD_{i_a} = 19.7\%$, $THD_{i_b} = 20.5\%$ and $THD_{i_c} = 19.5\%$. The harmonic spectrum of the currents during the fault are shown in Fig. 16.

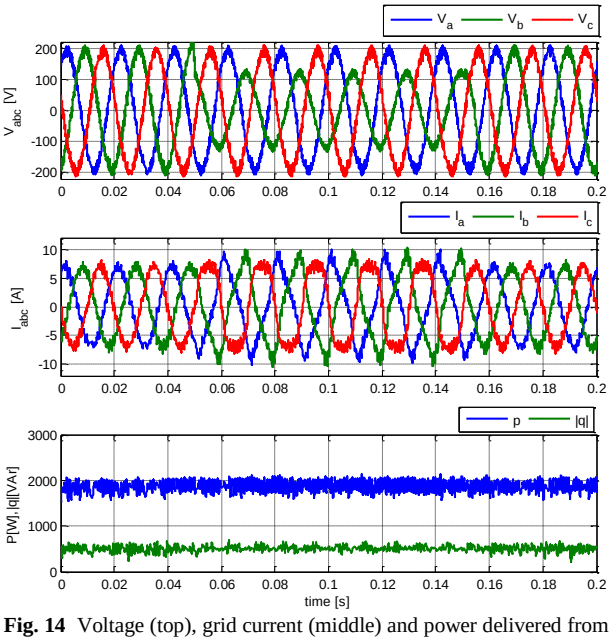

Fig. 14 Voltage (top), grid current (middle) and power delivered from PV panel (bottom) during voltage sag

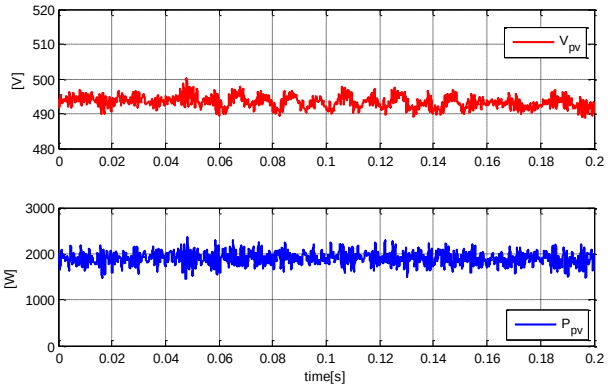

Fig. 15 Voltage (top), power for PV array (bottom) during voltage sag

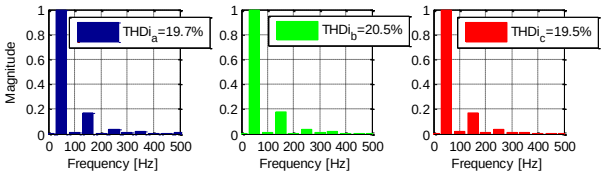

Fig. 16 Harmonic spectrum and THD for the currents during a sag

3.2 Voltage swell: 40% phase B

Fig. 17 shows the voltage, current and power of the system operating at MPP for 1000 W/m^2 and 25°C. The reactive power is set to zero. A running time of 0.2 s is considered for this experiment and a 40% voltage swell (Fig. 17 top) in phase B is applied from t=0.05s to t=0.15s. The grid fault has a zero-sequence voltage, hence the restriction in (10) is not fulfilled, and therefore only the active power can be regulated to its set-point. Fig. 17 (middle) shows the currents for the system. Under normal operation the RMS grid current is 4.7 A and 1.98 kW are injected to grid. During the swell the current reaches a 7.5 A peak, and the active power is kept at its reference value (1.98 kW). However, reactive power presents a ripple of 100 Hz with 300 VAr peak, see Fig. 17 (bottom).

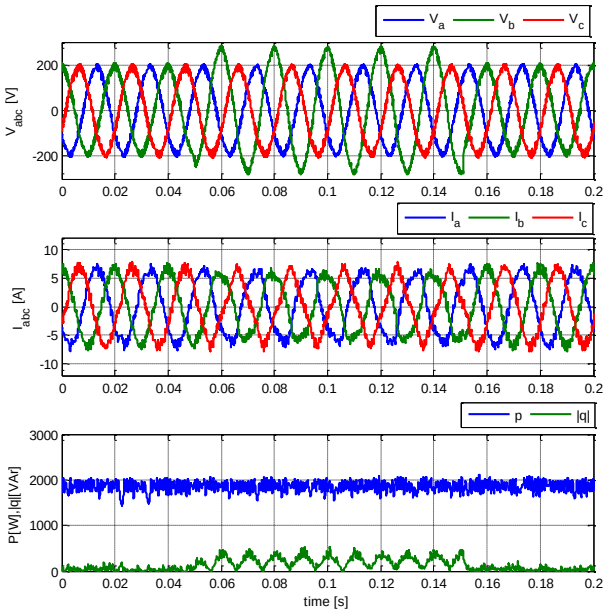

Fig. 17 Voltage (top), grid current (middle) and power delivered to the grid (bottom) during voltage swell

Fig. 18 shows the voltage and power delivered by the PV array during the voltage swell. Before the fault the PV array generates 2 kW at 495 V. During the fault the voltage has a 5 V and 100 Hz ripple whereas the PV power remains unchanged.

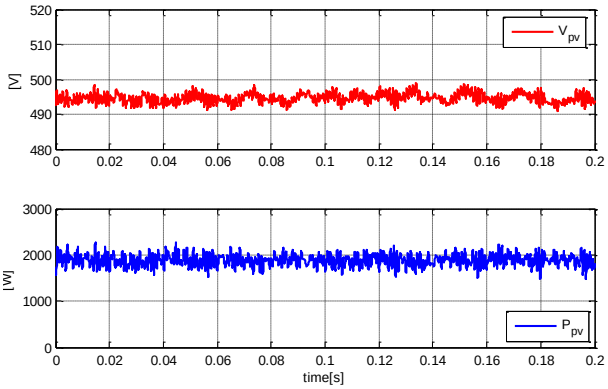

Fig. 18 Voltage (top), Power for PV array (bottom) during voltage swell

The harmonic spectrum of the currents during the fault are shown in Fig. 19 and the obtained THD values are: $THD_{i_a} = 16.8\%$, $THD_{i_b} = 14.7\%$ and $THD_{i_c} = 16.5\%$.

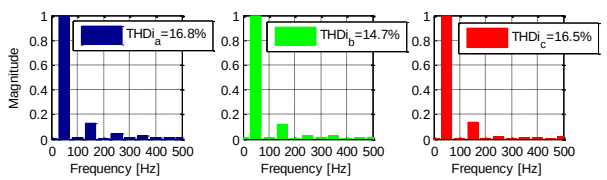

Fig. 19 Harmonic spectrum and THD for the currents during a swell

To regulate both active and reactive power under normal and fault conditions, the reactive power needs to be increased in order to satisfy (10). Considering an active

power of 1.98 kW and a 40% voltage swell, the minimum reactive power to satisfy (10) is 320 VAr. Therefore, the previous transient is repeated with a 325 VAr reactive power reference.

Fig. 20 shows the voltage, current and active/reactive power delivered to the grid during normal and fault conditions. The RMS pre-fault current is 4.73 A while the converter injects 1.98 kW and 325 VAr to the grid. During the grid fault active and reactive powers are regulated according to their reference values. Fig. 21 shows the voltage and power delivered from the PV array.

The string voltage ripple is similar than that of the transient with zero reactive power reference, whereas the control system keeps MPPT operation.

The currents harmonic spectrum obtained during the fault are shown in Fig. 22 and their THD values are: $THD_{i_a} = 16.8\%$, $THD_{i_b} = 15.7\%$ and $THD_{i_c} = 17.2\%$.

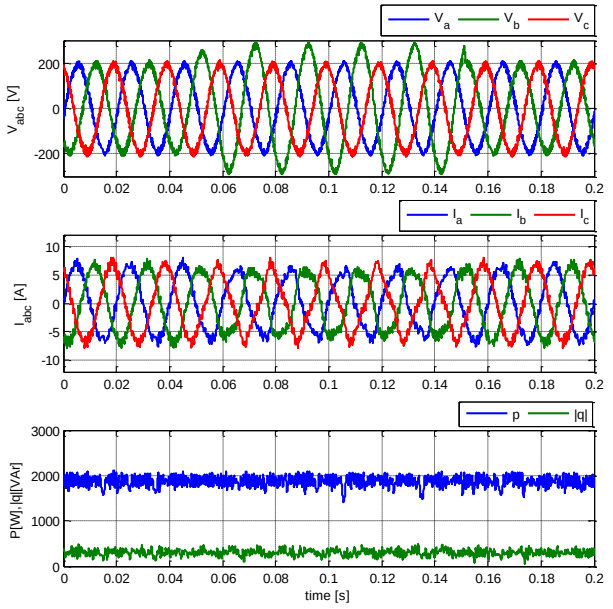

Fig. 20 Voltage (top), grid current (middle) and power delivered to the grid (bottom) during voltage swell

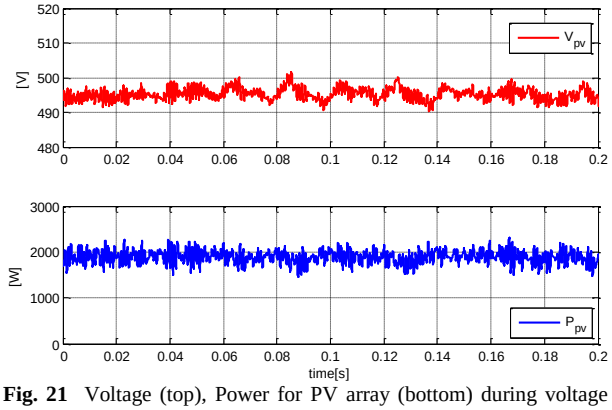

Fig. 21 Voltage (top), Power for PV array (bottom) during voltage swell

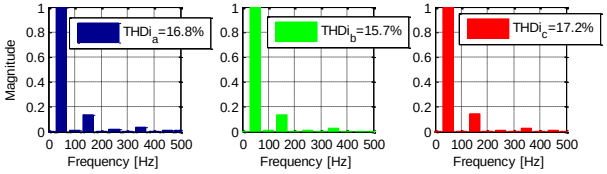

Fig. 22 Harmonic spectrum and THD for the currents during a swell

From all the experimental results shown, it is confirmed that the convergence to equilibrium during a fault is very fast (the response time is almost negligible). Moreover, although stability analysis is not the aim of this work, it is reasonable to state that since the PV generator keep constant the output power during a fault (and is not disconnected from the power system), it will not lead to voltage instability [40].

Considering some of the previous works, it can be mentioned that the results obtained for active/reactive power under asymmetrical sags and swells show a lower oscillation compared to the approach presented in [26] and a similar performance to the control scheme presented in [24] but with a much simpler implementation, making the proposed strategy promising for the current application.

On the other hand, regarding the *IEEE Standard for Interconnection and Interoperability of Distributed Energy Resources with Associated Electric Power Systems Interfaces* (IEEE Std 1547 - 2018) [41], the requirements under abnormal voltage conditions can be summarized in Fig. 23 [41].

From this figure, it is appreciable than the Distributed Energy Resource (DER) may ride-through or may trip if a phase voltage is lower than 0.5 pu or higher than 1.2 pu for a period lower to 0.16 s. For higher periods, the DER must trip. Moreover, for voltages in the range 0.5 - 0.7 pu there is a permissive operation capability area.

In the cases presented in this work, the faults experimented (voltage sag of 0.6 pu and voltage swell of 1.4 pu) have a duration of 0.1s and the system proposed ride-through, then complying with the requirements of the IEEE Std 1547.

Regarding islanding, also specified in the IEEE Std 1547, the DER shall detect the island and cease to energize within 2 s of the formation of an island. For the strategy presented in this paper, the system will actually be capable of detect an island and will cease to energize, as the reference current will be zero according to (8)-(9), without the presence of grid voltages. This action will last only one sampling period (56μ), then the system will comply with the unintentional islanding criteria.

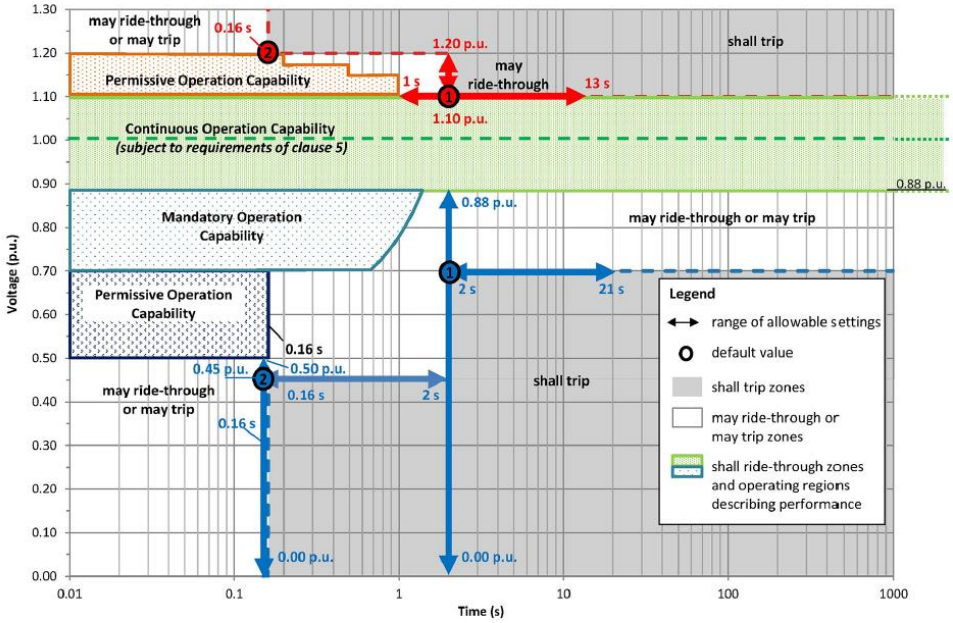

Fig. 23. DER response to abnormal voltages and voltage ride-through requirement

4 Conclusions

This paper has presented a theoretical analysis of a control strategy intended to supply a demanded active and reactive power from a PV system into the grid under balanced and unbalanced grid conditions. It has been shown that, under unbalanced grid voltage conditions, it is necessary to consider the magnitude of the voltage sag/swell, the active power and the zero-sequence voltage in order to regulate the reactive power flow between the inverter and the grid. The proposed strategy has been experimentally validated using an emulated PV panel. Several results have been shown and discussed for balanced grid operation and for grid voltage sags and swells, showing a good performance of the strategy proposed, compared to previous works, especially related to power steady state oscillations. Moreover, the response time of the proposed method is negligible, then the injected active and reactive power do not suffer noticeable variations during the fault (when the required restriction for q_{ref} is satisfied). On the other hand, the proposed strategy complies with the IEEE Std 1547 in terms of ride-through capability and islanding detection. Future work in this research line could include a thorough stability analysis with the PV system interacting with other generations sources (for instance in a hybrid microgrid) during fault conditions.

References

[1] Greentech Media Research “By 2023, the world will have 1 trillion Watts of installed solar PV capacity”. Available on https://www.greentechmedia.com/articles/read/by-2023-the-world-will-have-one-trillion-watts-of-installed-solar-pv-capaci.

[2] B. Subudhi and R. Pradhan, "A Comparative Study on Maximum Power Point Tracking Techniques for Photovoltaic Power Systems," in *IEEE Transactions on Sustainable Energy*, vol. 4, no. 1, pp. 89-98, Jan. 2013.

[3] Chih-Ming Hong, Ting-Chia Ou and Kai-Hung Lu, “Development of intelligent MPPT (maximum power point tracking) control for a grid-connected hybrid power generation system” in Energy, vol. 50, pp. 270-279, 2013.

[4] Ou Ting-Chia, H. Chih-Ming, “Dynamic operation and control of microgrid hybrid power systems,” in Energy, vol. 66, pp. 314-323, 2014.

[5] S. L. Prakash, M. Arutchelvi and S. S. Sharon, "Simulation and performance analysis of MPPT for single stage PV grid connected system," *Intelligent Systems and Control (ISCO), 2015 IEEE 9th International Conference on*, Coimbatore, 2015, pp. 1-6.

[6] A. Moghadasi, A. Sargolzaei, M. Moghaddami, A. I. Sarwat and K. Yen, "Active and reactive power control method for three-phase PV module-integrated converter based on a single-stage inverter," *2017 IEEE Applied Power Electronics Conference and Exposition (APEC)*, Tampa, FL, 2017, pp. 1357-1362.

[7] H. Li, Y. Xu, S. Adhikari, D. T. Rizy, F. Li and P. Irminger, "Real and reactive power control of a three-phase single-stage PV system and PV voltage stability," *2012 IEEE Power and Energy Society General Meeting*, San Diego, CA, 2012, pp. 1-8.

[8] R. Shao, R. Wei and L. Chang, "A multi-stage MPPT algorithm for PV systems based on golden section search method," *2014 IEEE Applied Power Electronics Conference and Exposition - APEC 2014*, Fort Worth, TX, 2014, pp. 676-683.

[9] J. W. Zapata, S. Kouro, M. Aguirre and T. Meynard, "Model predictive control of interleaved dc-dc stage for photovoltaic microconverters," *Industrial Electronics Society, IECON 2015 - 41st Annual Conference of the IEEE*, Yokohama, 2015, pp. 004311-004316.

[10] Dousoky, G. M., Ahmed, E. M., & Shoyama, M. “MPPT schemes for single-stage three-phase grid-connected photovoltaic voltage-source inverters”. In Industrial Technology (ICIT), 2013 IEEE International Conference. pp. 600-605. Feb. 2013.

[11] Electricity System Operator (ESO) webpage: www.nationalgrideso.com.

[12] A. Al-Shetwi, M. Sujod, F. Blaabjerg and Y. Yang, “Fault ride-through control of grid-connected photovoltaic power plants: A review,” in Solar Energy, vol. 180, pp. 340-350, 2019.

[13] P. Almeida, K. Monteiro, P. Barbosa, J. Duarte and P. Ribeiro, “Improvement of PV grid-tied inverters operation under asymmetrical fault conditions,” in Solar Energy, vol. 133, pp. 363-371, 2016.

[14] G. Ding, F. Gao, H. Tian, C. Ma, M. Chen, G. He, Y. Liang, “Adaptive DC-link voltage control of two-stage photovoltaic inverter during low voltage ride-through operation” in *IEEE Transactions on Power Electronics*, vol. 31, pp. 4182-4194, 2016.

[15] J. Miret, M. Castilla, A. Camacho, L. G. d. Vicuña and J. Matas, "Control Scheme for Photovoltaic Three-Phase Inverters to Minimize Peak Currents During Unbalanced Grid-Voltage Sags," in *IEEE Transactions on Power Electronics*, vol. 27, pp. 4262-4271, 2012.

[16] S. Naderi, M. Negnevitsky, A. Jalilian and M. Hagh, “Efficient fault ride-through scheme for three phase voltage source inverter-interfaced distributed generation using DC link adjustable resistive type fault current limiter,” in Renewable Energy, vol. 92, pp. 484-498, 2016.

[17] A. Merabet, L. Labib and A. M. Y. M. Ghias, "Robust Model Predictive Control for Photovoltaic Inverter System With Grid Fault Ride-Through Capability," in *IEEE Transactions on Smart Grid*, vol. 9, pp. 5699-5709, 2018.

[18] Ou Ting-Chia, “A novel unsymmetrical faults analysis for microgrid distribution systems,” in Electrical Power and Energy Systems, vol. 43, pp. 1017-1024, 2012.

[19] W. Lin and T. Ou, "Unbalanced distribution network fault analysis with hybrid compensation," in *IET Generation, Transmission & Distribution*, vol. 5, pp. 92-100, 2011.

[20] Ou Ting-Chia, “Ground fault current analysis with a direct building algorithm for microgrid distribution,” in Electrical Power and Energy Systems, vol. 53, pp. 867-875, 2013.

[21] Ou Ting-Chia, Lu Kai-Hung and Huang Chiou-Jye, “Improvement of transient stability in a hybrid power multi-system using a designed NIDC (Novel Intelligent Damping Controller)” in Energies, vol. 10, 2017.

[22] I. Sadeghkhani, M. Hamedani, J. Guerrero and Ali Mehrizi-Sani, “A Current Limiting Strategy to Improve Fault Ride-Through of Inverter Interfaced Autonomous Microgrids” in IEEE Transactions on Smart Grid, vol. 8, pp. 2138-2148, 2017.

[23] A. Junyent-Ferre, O. Gomis-Bellmunt, T. Green, and D. Soto-Sanchez, “Current control reference calculation issues for the operation of renewable source grid interface VSCs under unbalanced voltage sags,” IEEE Transactions on Power Electronics, vol. 26, no. 12, pp. 3744–3753, Dec. 2011

[24] M. Castilla, J. Miret, J. L. Sosa, J. Matas, and L. G. de Vicuña, “Grid-fault control scheme for three-phase photovoltaic inverters with adjustable power quality characteristics,” Power Electronics, IEEE Transactions on, vol. 25, no. 12, pp. 2930–2940, 2010.

[25] Camacho, A., Castilla, M., Miret, J., Vasquez, J. C., & Alarcón-Gallo, E. "Flexible voltage support control for three-phase distributed generation inverters under grid fault." Industrial Electronics, IEEE Transactions on vol. 60 no. 4, pp. 1429-1441. 2013.

[26] Sosa, J. L., Castilla, M., Miret, J., Matas, J., & Al-Turki, Y. A."Control Strategy to Maximize the Power Capability of PV Three-Phase Inverters During Voltage Sags." Power Electronics, IEEE Transactions on 31.4, 2016, pp 3314-3323.

[27] Lin, Faa-Jeng, et al. "Reactive Power Control of Three-Phase Grid-Connected PV System during Grid Faults Using Takagi-Sugeno-Kang Probabilistic Fuzzy Neural Network Control” IEEE transactions on industrial electronics, vol. 62, No. 9, September 2015, pp 5516-5528.

[28] G. Hunter, I. Andrade, J. Riedemann, R. Blasco-Gimenez and R. Peña, "Active and reactive power control during unbalanced grid voltage in PV systems," *IECON 2016 - 42nd Annual Conference of the IEEE Industrial Electronics Society*, Florence, 2016, pp. 3012-3017.

[29] J. Rodrıguez, J. Pontt, C. A. Silva, P. Correa, P. Lezana, P. Cortes, and U. Ammann, “Predictive current control of a voltage source inverter,” Industrial Electronics, IEEE Transactions on, vol. 54, no. 1, pp. 495– 503, 2007.

[30] M. B. Shadmand, R. S. Balog and H. Abu-Rub, "Model Predictive Control of PV Sources in a Smart DC Distribution System: Maximum Power Point Tracking and Droop Control," in *IEEE Transactions on Energy Conversion*, vol. 29, no. 4, pp. 913-921, Dec. 2014.

[31] M. Lei *et al*., "An MPC-Based ESS Control Method for PV Power Smoothing Applications," in *IEEE Transactions on Power Electronics*, vol. 33, no. 3, pp. 2136-2144, March 2018.

[32] I. Hussain and B. Singh, "Grid integration of large capacity solar PV plant using multipulse VSC with robust PLL based control," *Power India International Conference (PIICON), 2014 6th IEEE*, Delhi, 2014, pp. 1-6.

[33] G. Bayrak, E. Kabalci and M. Cebecı, "Real time power flow monitoring in a PLL inverter based PV distributed generation system," *Power Electronics and Motion Control Conference and Exposition (PEMC), 2014 16th International*, Antalya, 2014, pp. 1035-1040.

[34] U. P. Yagnik and M. D. Solanki, "Comparison of L, LC & LCL filter for grid connected converter," *2017 International Conference on Trends in Electronics and Informatics (ICEI)*, Tirunelveli, 2017, pp. 455-458.

[35] A. K. Gupta and R. Saxena, "Review on widely-used MPPT techniques for PV applications," *2016 International Conference on Innovation and Challenges in Cyber Security (ICICCS-INBUSH)*, Noida, 2016, pp. 270-273.

[36] Schmidt, H., Burger, B., Bussemas, U., & Elies, S. “How fast does an MPP tracker really need to be?”. Proc. of 24th EuPVSEC, pp. 3273-3276. 2009

[37] Abu-Rub, Haitham, Mariusz Malinowski, and Kamal Al-Haddad. Power electronics for renewable energy systems, transportation and industrial applications. John Wiley & Sons, 2014.

[38] J. Rodriguez and P. Cortes, Predictive control of power converters and electrical drives, vol. 37. John Wiley & Sons, 2012.

[39] Peng, Fang Zheng, and Jih-Sheng Lai. "Generalized instantaneous reactive power theory for three-phase power systems”, Instrumentation and Measurement, IEEE Transactions vol. 45 no. 1, pp. 293-297, 1996.

[40] Y. Mitsugi and A. Yokoyama, "Phase angle and voltage stability assessment in multi-machine power system with massive integration of PV considering PV's FRT requirements and dynamic load characteristics," *2014 International Conference on Power System Technology*, Chengdu, 2014, pp. 1112-1119.

[41] IEEE-SA Standards Board, “IEEE Standard for Interconnection and Interoperability of Distributed Energy Resources with Associated Electric Power Systems Interfaces” (IEEE Std 1547), 2018.